Mitochondria form cholesterol-rich contact sites with the nucleus during retrograde response

Radha Desai[1*], Daniel A East[1*], Liana Hardy[1], James Crosby[1], Danilo Faccenda[1], María Soledad Alvarez[1], Marta Mainenti[1], Laura Kuhlman Hussey[1], Robert Bentham[2], Gyorgy Szabadkai[2,3,4], Valentina Zappulli[5], Roland A. Fleck[6], Gema Vizcay-Barrena[6], Gurtej Dhoot[1], Kenneth Smith[7] and Michelangelo Campanella[1,2]

[1]Department of Comparative Biomedical Sciences, The Royal Veterinary College, University of London, Royal College Street NW1 0TU, London, United Kingdom; [2]Department of Cell and Developmental Biology, Consortium for Mitochondrial Research (CfMR), University College London, Gower Street, WC1E 6BT, London, UK; [3]Department of Biomedical Science, University of Padua, Via Ugo Bassi, 35131, Padua, Italy; [4]Francis Crick Institute, Midland Road, NW1 AT, London, UK; [5]Department of Comparative Biomedicine and Food Sciences, University of Padua, Viale G. Colombo, 35121 Padua, Italy; [6]Centre for Ultrastructural Imaging, King's College London, London SE1 1UL, UK; [7]Pathobiology and Population Sciences, The Royal Veterinary College, Hawkshead Lane, North Mymms, Hatfield, Hertfordshire, AL9 7TA UK

*The authors wish to acknowledge RD and DE as equal contributors

To whom correspondence should be addressed:

Michelangelo Campanella

Email: mcampanella@rvc.ac.uk

Royal College Street, London, NW1 0TU, UK

Abstract

Cholesterol metabolism is pivotal to cellular homeostasis, hormones production, and membranes composition. Its dysregulation associates with malignant reprogramming and therapy resistance. Cholesterol is trafficked into the mitochondria for steroidogenesis by the transduceome protein complex, which assembles on the outer mitochondrial membrane (OMM). The highly conserved, cholesterol-binding, stress-reactive, 18kDa translocator protein (TSPO), is a key component of this complex. Here, we modulate TSPO to study the process of mitochondrial retrograde signalling with the nucleus, by dissecting the role played by cholesterol and its oxidized forms. Using confocal and ultrastructural imaging, we describe that TSPO enriched mitochondria, remodel around the nucleus, gathering in cholesterol-enriched domains (or contact sites). This communication is controlled by HMG-CoA reductase inhibitors (statins), molecular and pharmacological regulation of TSPO. The described Nucleus-Associated Mitochondria (NAM) seem to be implementing survival signalling in aggressive forms of breast cancer. This work therefore provides the first evidence for a functional and biomechanical tethering between mitochondria and nucleus, as being the basis of pro-survival mechanisms, thus establishing a new paradigm in cross-organelle communication via cholesterol re-distribution.

Key words: mitochondria, cholesterol, TSPO, cancer and contact sites

Key Messages

- **Pathological alteration of cholesterol metabolism and upregulation of mitochondrial 18kDa Translocator Protein expression triggers a pro-survival retrograde response;**
- **This operates via physical interaction between remodelled mitochondria and the nucleus via cholesterol-rich domains;**
- **Lowering cholesterol as well as chemical targeting of TSPO control the cholesterol driven efficacy of this pro-survival mitochondria to nucleus signalling;**

Introduction

Mitochondria actively take part in remodelling and reprogramming of mammalian cells. In response to stressors, either of endogenous or exogenous nature, they retro-communicate with the nucleus to induce wide-ranging cytoprotective effects that sustain proliferation and death evasion. This process, which goes under the name of mitochondrial retrograde response (MRR) and exploited in pathological settings, is driven by deregulation of Reactive Oxygen Species (ROS), Ca^{2+} signalling and energy defects that promote nuclear stabilization of transcription factors (e.g. nuclear factor kappa-light-chain-enhancer of activated B cells, NF-kB), responsible to drive the metabolic rewiring and resistance mechanisms to therapy. In hormone-dependent tumours, such as those of the mammary gland, the therapeutic failure of therapy is now linked to alterations in the cholesterol metabolism[1,2]. The 18kDa mitochondrial protein TSPO[3], which trasnlocates cholesterol from the outer into the inner mitochondrial environment, is overexpressed in these pathologies which it might contribute by impacting their MRR[4,5] via core features of its recently enlighten molecular physiology[5],[6].

The retrograde (mitochondria to nucleus) communication[7] is indeed driven by mitochondrial dysfunction[8-11] which associates with TSPO overexpression as this leads to intracellular redox-stress (ii), raised cytosolic Ca^{2+} transients (iii), and organelle compartmentalization of cholesterol (iii). The metabolic rewiring[12] which is a key step in the cancerous transformation[13,14] is therefore secondary to deregulated mitochondrial function. Cholesterol and cholesterol-derived intermediates have been instead recently highlighted as a determinant in the oncogenic reprogramming[1]. Metastatic, endocrine therapy breast cancer cells, isolated from patients, show increased expression of CYP19A1, a member of the cytochrome C p450 monooxygenase enzymes[2], which catalyses the last steps of oestrogen synthesis from cholesterol. This prompted the curiosity for the contribution cholesterol-associated proteins such as TSPO could play in this process and how mitochondrial

trafficking of cholesterol could influence the MRR. TSPO which localises on the Outer Mitochondrial Membrane (OMM) is detected at greater levels in the aggressive forms of the mammary lesions[15-17], and besides taking part in the synthesis the steroids by shuttling cholesterol[18-20] into the mitochondria its also impairs mitophagy[21,22] resulting in poor organelle respiration and handling of Ca^{2+}[22,23]. Notably, TSPO is reported of anti-apoptotic activity[24] and its ligands tested as chemotherapy co-adjuvant[25] as well as PET-biomarkers of metastases[26,27]; however its role in the management of cholesterol and the MRR in the economy of cellular pathophysiology remains unexplored. Cholesterol synthesis inhibition improves mitochondrial driven apoptosis of cancer cells[28] but whether influences the efficacy of MRR is untested. The driving hypothesis for this work was therefore that in response to stressors cholesterol accumulates on the outer mitochondrial membrane (OMM) via TSPO priming mitochondria retrograde communication with the nucleus via the formation of cholesterol-rich domains which facilitate stabilization of pro-survival transcription factors[29]. Using a combination of imaging methods at cellular and ultrastructural level along with pioneering protocols of cholesterol dynamics analysis we are here detailing a molecular axis of communication between mitochondria and nucleus (i), provide evidences for hot-spots which link mitochondria with nucleus (ii) and to biochemically and pharmacologically control this route of signalling via the protein target TSPO (iii).

Results

The association between TSPO and NF-kB was initially corroborated in primary human samples of mammary gland tumours in which we observed a positive correlation between TSPO expression and the aggressiveness of the lesions (**Figure 1 a, b**) mirrored by the pattern of NF-κB[29,30] accumulation in the nucleus (**Figure 1d, e**). In agreement with this, transcriptomic analysis of >600 samples of breast cancer in the Cancer Genome Atlas (TCGA) showed higher NF-κB mRNA expression in the more aggressive HER positive and basal tumours which correlated mRNA expression of TSPO (**Figure 1c, f**) without detection of any mutation (**SFigure 1a**). The positive correlation between the highly conserved (**SFigure 1d**) TSPO, and aggressiveness of neoplastic conditions of the mammary gland is therefore retained across species (**SFigure 1e-g**).

In order to elucidate the nature of this oncogenic capacity we moved the analysis to cell lines of human breast cancer[15] and interrogated the biochemical mechanisms responsible for the interplay between NF-κB nuclear translocation and mitochondrial expression of TSPO. We compare epithelial human breast cancer MCF-7 cells which features low TSPO levels and a more aggressive counterpart MDA-MB-231 (henceforth referred to as MDA) derived from breast cancer adenocarcinoma which instead express high levels of TSPO[3] (**Figure 1g-i**). In MDA, TSPO was then knocked down (**SFigure 1b**) before exposing the cohorts of cells (with high and low TSPO) to Staurosporine (STS), used here as a mitochondrial stressor/apoptotic stimulus, and we observed an increase in TSPO expression as a reaction to the stressor (**SFigure 1c**). Application of STS led to nuclear translocation of NF-κB, which was tangibly reduced in those cells with reduced TSPO expression (**Figure 1j, k**). The same pattern was seen in the expression of NF-κB-regulated pro-survival genes Bcl-2 and c-FLIP (**Figure 1l, m**). Immunocytochemical analysis further highlighted the degree of nuclear translocation of the NF-κB upon STS treatment in presence of TSPO-expressing mitochondria and how pruning of the mitochondrial network via pharmacological activation of mitophagy via the

agent PMI[31,32] reduced the efficacy of NF-κB translocation (**Figure 1n, o**). PMI, which we confirmed is able to reduce size of the mitochondrial network as well as the expression of TSPO (**SFigure 1j**), sensitizes human, feline and canine breast cancer cells to STS-induced apoptosis (**SFigure 2k-m**). Suggesting that the mass of the mitochondrial network is important in facilitating the transcriptomic capacity of NF-κB. Notably also, is the ability of TSPO ligand PK11195 (which targets the cholesterol binding domain of the protein[33]) reduced the nuclear translocation of NF-kB when combined with STS (**Figure 2a, b**). Furthermore, the cholesterol synthesis inhibitor, pravastatin (PVS) also reduces NF-κB translocation suggesting that the TSPO-cargo cholesterol, is likely to precipitate the Mitochondrial Retrograde Response induced nuclear translocation of NF-kB **(Figure 2c).** Confirmation of the interaction between TSPO, Cholesterol and NF-κB was elucidated by MDA cells constitutively knocked-out of NF-κB in which further outcome on STS induced cell death was exercised by the concomitant repression of TSPO (**Figure 2d**). NF-kB competent MDA are susceptible to the changes in TSPO expression as well as treatment with its ligands. TSPO deficient MDA cells ($TSPO^{-}$) have therefore increased: i) sensitivity to apoptosis (**Figure 2e**), ii) proliferative capacity (**Figure 2f**), iii) accumulation of the pro-apoptotic molecule BAX on their mitochondria (**Figure 2 g, h**) and iv) Cytochrome C release into the cytosol (**Figure 2i, j**). TSPO ligands (See **Table 2**) substantially increase susceptibility to STS (**Figure 2k**), Doxorubicin and Vincristine induced cell death (**Figure 2l-m**).

MCF-7 cells, which constitutively express lower TSPO levels, gain resistance to STS-Induced apoptosis, when the gene is overexpressed but solely when the recombinant wild-type isoform of the protein is inserted, whereas, the mutant lacking the Cholesterol Binding Domain CRAC (TSPOΔCRAC) fails confer this resistance (**Figure 3a-c**). This evidence further demonstrates that is the cholesterol-binding capacity of TSPO is key to cellular resistance to chemically induced cell death. Furthermore, MCF-7 cells which have

developed resistance to Tamoxifen due to their increased cholesterol bio-synthesis in response to long-term oestrogen deprivation, (MCF7-LTED [1,34,35]) present a high expression of TSPO (**Figure 3d, e**). On the basis of this evidence we investigated whether pharmacological targeting of TSPO with FGIN-127 ligand could affect the nuclear pattern of the ERα in MCF7-LTED and their susceptibility to STS induced cell death. In both these parameters, the ligands was effective resulting in reducing ERα association with the nucleus (**Figure 3g)** and higher cell death (**Figure 3h).** Aligning with these observations, big-data analysis revealed that TSPO is over-expressed in cohorts of relapsed patients in whom endocrine therapy was no longer effective and cholesterol metabolism is escalated. (**Supplementary Figure 3 a**).

Following co-immunocytochemical labelling of TSPO and the nuclear envelope protein Lamin-B we report that in MDA but not in MCF-7 cells, mitochondria are persistent in the perinuclear region forming an association with the nucleus similar to an infiltration (**Figure 4a,b**). This increases in response to STS and is concurrent with the retro-translocation of TSPO into the nucleus (**Figure 4c, d**). The degree of nuclear association of mitochondria (nucleus-associated mitochondria: NAM) is enhanced by STS, and this can be limited by the mitophagy-driven reduction of the mitochondrial network when co-treated with PMI (**Figure 4e- g**). TSPO trafficking into the nucleus was confirmed by immunogold staining followed by Transmission Electron Micrograph (TEM) where TSPO was observed to be present in mitochondrial OMM, nuclear envelope, as well as inside the nucleus. Also ultrastructural imaging revealed the inter-organellar coupling which establishing the NAM as an all-encompassing structure in and around the nucleus (**Figure 4h, i**).

The observed mitochondrial remodelling could crucially influence the efficiency of signalling via diffusible molecules such as ROS which are acknowledged activators of the retrograde response[36] and increased both in mitochondrial and cytosolic compartments according to TSPO expression (**Figure 4j-l**) as shown in precedence.

Further TEM analysis confirmed that remodelled mitochondria, in response to cell challenge by STS, converge into the peri and intra- nuclear region promoting a large change in the median distance with the centre of the nucleus (**Figure 4 m, Supplementary Figure 2 a. b**). We have ascertained such a change in shortening of the distance between mitochondria and the nucleus of 4.3μm (please refer to **Table 1**) between untreated and treated conditions as graphically represented in **Figure 4 n**). Confirmation of NAM as a means to assess the inter-organelles coupling was corroborated in Mouse Embryonic Fibroblasts (MEFs) transiently overexpressing TSPO, in which hot-spots of contact between mitochondria and nucleus are appreciable (**Figure 4 o**). $TSPO^{++}$ MEFs are also resistant to STS induced cell death (**Figure 4 p**) showing greater retention of cholesterol in the nuclear environment (**Figure 4 q**). Most notably, this occurs following overexpression of the wild type TSPO whilst its mutant isoform ΔTSPO-CRAC mediates neither protection nor cholesterol retention during STS treatment.

Reducing the distance between mitochondria and nucleus could be important to other signalling effectors downstream of impaired redox-stress and cholesterol metabolism. Localized pools of ROS on the nucleus may lead to greater oxidation of the cholesterol tethered by TSPO, thus establishing a relay between TSPO, cholesterol and ROS via the generation of oxysterols that underlie various conditions including malignant proliferation[37,38]. In keeping with this, exposure of MDA to 7-ketocholesterol (7 KC) (which is the second most abundant oxysterol found in mammals) increases TSPO expression (**Figure 5 a-c**) and re-enforces the NAM (**Figure 5 d, e**). The same pattern of expression is mirrored by LXR-β, ATAD3 and StAR (**SFigure 2d-h**), all of which are components of the steroidogenic protein complex- transduceome[19]. Subsequently, in Mito-RFP expressing MDA cells co-labelled for Lamin B we imaged cholesterol pools via the cholesterol-binding fluorescent compound, Filipin observing their localization into focal spots on the nucleus following STS treatment which were instead prevented when TSPO expression was reduced (**Figure 5f,**

g). STS thus triggers a re-distribution of cholesterol out of the nucleus, which is already occurring in cells with reduced TSPO expression (**Figure 5h**) or treated with ligands of the protein (**Figure 5i**). This goes in line with the reduced expression of NF-κB regulated pro-survival genes (c-FLIP, Bcl-2) recorded when MDA are treated with Lovastatin (**Figure 5j, k**) thus confirming the accumulation of cholesterol into the nucleus is pivotal for the transcription of pro-survival genes at the basis of Mitochondrial Retrograde Response (MRR). We also confirmed that pharmacological regulation of TSPO affects cholesterol dynamics by imaging the process with the fluorescent dye dehydroergosterol (Ergosta): a cholesterol surrogate[39]. By measuring the threshold percentage area of the Ergosta signal co-localized with mitochondria (demarked by Mitotracker Red) we reported that the TSPO ligand PK11195, prevents the invasion of the nuclear region by the lipid leaving this compartmentalised in the mitochondria (**Figure 5l, m)** which also present a more arborized network following the treatment (**Figure 5 n,o**). The conclusions of this evidence, are summarised in the final graphical model (**Figure 5p**) in which we highlight that the association of mitochondria with the nucleus relies on cholesterol-rich domains demarked, at least in our experimental model by TSPO which is therefore useful both for their traceability and regulation.

Discussion

The characterization of molecular effectors in the mitochondrial retrograde communication with the nucleus is instrumental in understanding the origin of mammalian cells adaptation to stress and pro-pathological cues. In this work, we demonstrate that this conduit of communication relies on spatially confined biochemical events, secondary to remodelling of mitochondria that can associate with the nucleus. Localized accumulation of cholesterol is pivotal to this and in promoting expression of pro-survival genes. Hitherto, just the Reactive Oxygen Species (ROS) and Ca^{2+} were acknowledged[7,11] pro-survival messengers operating between mitochondria and nucleus whilst we prove that cholesterol operates as an intermediate of equal if not greater relevance in this conduit of communication.

Dissipation of cholesterol from the nucleus emerges therefore as an indicator of the degree of successful apoptosis whilst its retention of the very opposite. This is not surprising, though, as cholesterol is known to be involved in the expression of genes by stabilizing their transcription[40]. However, discovery that cholesterol is trafficked via hot-spots at the interface between the organelles is truly novel even though similar to other communication platforms such as ER-MAMs.

In malignant models of analysis presenting altered cholesterol metabolism such as the MDA the association between Mitochondria and the Nucleus which we called NAM (Nucleus-Associated Mitochondria) results in greater exposure of the nucleus to hydrogen peroxide (H_2O_2), superoxide (O_2^-) as well as hydroxyl radical (OH^-) generated in excess by defective mitochondria -as happen to occur in those overexpressing TSPO. That mitochondrial O_2^- and OH^- can travel for less than a micron in their very short half-life (represented in **Figure 4n)** (which can be estimated based on their diffusion co-efficient[41]) prevents these reactive species from causing excessive damage or uncontrolled signalling in steady state. However, the formation of NAM, by bringing mitochondria within angstroms range with the nuclear DNA, will facilitate the efficient transmission of these molecules[36]. NAM will equally benefit

the stabilization in the nucleus of transcriptional factor such as NF-κB[11] boosting the transcription of the regulated pro-survival genes. In this manner, NAM may represent a defensive mechanism in response to apoptotic cues in the short term, whilst long-term exposure of the nucleus to free radicals, will compromise DNA integrity leading to genomic alterations. This ties well into observations that cytoskeletal reorganization and cellular morphology are key factors in determining the cellular resistance to apoptosis as well as in regulating the NF-κB led signalling[42,43]. Equally, nuclear pleomorphism of tumours which is proposed as a biomarker of malignancy for breast cancer[44], could be due to the continuous exploitation of this mechanism thus resulting in resistance generating somatic mutations.

We report that in response to pro-apoptotic stressors mitochondria re-organise and overwhelm the nuclear envelope. OMM based proteins such as TSPO, may even being trafficked into the nucleus delivering their lipid cargo (e.g. cholesterol). The putative concurrence of ROS in the nucleus along with cholesterol implies that auto-oxidative products of cholesterols (oxysterols) may be also involved in the signalling route and the pattern of LRX receptors[19], mirroring that of TSPO, stands as confirmation. All this is nonetheless secondary to inefficient mitochondrial quality control, which accumulates inefficient organelles and their bypassed respiratory products. TSPO suppresses PINK1-PARKIN driven mitophagy by impairing the ubiquitination of proteins[21]. The mitochondria which overexpress TSPO are therefore far more prone to repositioning, as systematically evading control by autophagy, increasing nuclear stabilization of the NF-κB. A correlation which is retained cross the aggressive cell lines investigated as well as the histopathological samples (both of human and non-human origin) analysed.

The previously described de-ubiquitinating properties of TSPO[22], lead us to speculate that trafficking of TSPO onto the nuclear envelope could replicate a similar inhibitory role for the nucleophagy in dying cells and the undulated nuclear envelope we observe ultrastructurally could be consequence of this. However, the alteration in lipid composition of the membranes

to which TSPO localises (mitochondria) or relocalises (nucleus) may be key to this as well as to the altered organellar life cycle and interactome. Certain is that Mitochondrial network remodelling, cholesterol sequestration on the perinuclear region and cell death evasion are all avoidable by downregulation of TSPO or its pharmacological counteraction via PK11195, FGN-127. TSPO is thus further overexpressed in mammary gland cell lines that have developed resistance to Endocrine Therapy (ET). Its recombinant overexpression confers resistance to those cells still susceptible to ET whilst the ΔTSPO-CRAC mutant unable to bind and collect cholesterol fails to mediate similar outcome. These experiments confirm therefore a critical role for the TSPO cargo cholesterol in the regulation of MRR, which is executed both by physical re-organization of the mitochondrial network on the nucleus and accumulation of cholesterol in specific domains. These findings shed new light on the resistance behaviour primed by MRR providing a mechanistic base which occurs via the regulation of cholesterol.

While the observation that the mitochondrial interactome is crucial to cellular health is not new, here we suggest, that what has previously been simply described as perinuclear arrangement of mitochondria, has deeper consequences for molecular signalling, cellular health and survival. Furthermore, we identify cellular conditions of stress where the interaction can be controlled and is exploited for cell survival. Amongst the family of intracellular organelles, mitochondria are particularly dynamic. In particular, their ability to communicate with the nucleus, is not just intraorganellar communication, but a conversation strategy between two genomes to retain homeostasis. And it is no coincidence that an highly conserved and ancient protein as TSPO emerges as core to this.

Author Contribution

M.C. conceived, designed and coordinated the project together with R.D, and D.A.E. M.C. R.D., L.H., D.A.E, J.C., D.F., M. S. A. performed the experiments and ran the analysis. R.F., G.V and L.A performed the EM analysis whilst G. T., M.M. the immunohistochemistry analysis on which guidance was obtained by K.S and V.Z., R.B. and G.S. worked out the bioinformatics data.

All authors have critically reviewed the manuscript and advised accordingly.

Acknowledgments

The research activities lead by M.C. are supported by the following funders, who are gratefully acknowledged: Biotechnology and Biological Sciences Research Council [grant numbers BB/M010384/1 and BB/N007042/1]; Bloomsbury Colleges Consortium PhD Studentship Scheme; The Petplan Charitable Trust; Umberto Veronesi Foundation; Marie Curie Actions and LAM-Bighi Grant Initiative. FIRB-Research Grant Consolidator Grant 2 [grant number: RBFR13P392], Italian Ministry of Health [IFO14/01/R/52].

Conflict of Interest

This research was conducted in the absence of any commercial or financial relationships that could be construed as a potential conflict of interest.

Methods

Immunohistochemistry/Immunocytochemistry*:* Immunofluorescence: Cells were fixed in 4% PFA (10 mins, RT) followed by 3 five-minute washes in PBS. Permeabilization was performed with 0.5% Triton-X in PBS (10 mins, RT) followed by washing. Blocking was carried out for 1h at RT in 10% Goat Serum and 3% BSA in PBS. Primary antibody incubations were conducted overnight for 16 h at 4˚C in blocking solution as described. After a further wash step, secondary antibodies were incubated for 1 h in blocking solution, before a final wash step. Cells were then mounted on slides with DAPI mounting medium (Abcam, ab104139). Cells were stained with the following primary antibodies: ATPB (Abcam ab14730) 1:400, Lamin B2 (Abcam ab8983) 1:500; TSPO (Abcam, ab109497)

1:200, NF-kB (AbCam, ab16502) 1:500, 1:1000 ATAD3 (Gift from Dr Ian Holt, Biodonista, 1:400 LXRβ (Abcam ab28479), 1:500 STAR (AbCam ab58013); and the following secondary antibodies: α-mouse Alexa 555 (Life Technologies, A21424) 1:1000; α-rabbit Alexa 488 (Life Technologies, A11008) 1:1000.

Single dye immunofluorescence was used to stain paraffin sections of human mammary tissues with different TSPO antibody (ab109497) / NF-kB (ab32360)

. The binding of mouse primary antibodies was detected using Alexa Fluor 488 (or 594) fluorochrome-conjugated goat anti-mouse IgG. Tissue sections were mounted with Floroshield Mounting Medium with DAPI to show

***Cell Culture**:* Human mammary cell lines MDA-MB-231 and MCF7 canine mammary line CF41 and feline mammary line K248P, were maintained at 37˚C under humidified conditions and 5% CO_2 and grown in Dulbecco's modified Eagle medium (Life Technologies, 41966-052) supplemented with 10% foetal bovine serum (Life Technologies, 10082-147), 100 U/mL penicillin, and 100 mg/mL streptomycin (Life Technologies, 15140-122). K248P cells were additionally supplemented with 10 µg/ml insulin (sigma-aldrich). Cells were transiently transfected with genes of interest or siRNA using a standard Ca^{2+} phosphate method as described previously [45] or using manufacturers' instructions for Lipofectamine 3000 (Thermofisher 18324010).

***Cell Fractionation**:* Cells were lysed in cold isotonic buffer (250 mM Sucrose, 10 mM KCl, 1.5 mM $MgCl_2$, 1 mM EDTA, 1 mM EGTA, 20 mM HEPES, pH 7.4) containing protease inhibitor cocktail (Roche, 05892791001) by passing through a 26-gauge needle 10 times using a 1 ml syringe, followed by 20 minutes incubation on ice. Nuclei were separated by centrifugation at 800g for 5 minutes at 4°C. For nuclear fractions, pellets were washed once in isotonic buffer followed by centrifugation 800g for 10 minutes at 4°C. Pellets were suspended in standard lysis buffer (150 mM NaCl, 1% v/v Triton X-100, 20 mM Tris pH 7.4) plus 10% glycerol and 0.1% SDS and sonicated for 5 seconds to dissolve pellet. For

mitochondrial fractions, supernatants were transferred to fresh tubes and centrifuged at 10000g for 10 minutes at 4°C, Subsequent supernatants were collected as the cytosolic fractions while mitochondrial pellets were washed once in cold isotonic buffer then centrifuged at 10000g for 10 minutes at 4°C. Finally, mitochondrial pellets were lysed in lysis for 30 minutes on ice.

Western Blot*:* Sample proteins were quantified using a BCA protein assay kit (Fisher Scientific, 13276818). Equal amounts of protein (10-30 µg for whole cell lysates/cytosolic fractions; 10 µg for mitochondrial. Nuclear fractions) were resolved on 12% SDS-PAGE gels and transferred to nitrocellulose membranes (Fisher Scientific, 10339574). The membranes were blocked in 3% non-fat dry milk in TBST (50 mM Tris, 150 mM NaCl, 0.05% Tween 20, pH 7.5) for 1 h then incubated with the appropriate diluted primary antibody at 4˚C overnight: LC3 (Abcam, ab48394) 1:1000; TSPO (Abcam, ab109497) 1:5000; Actin (ab8266). 1:2000; ATPB (Abcam, ab14730) 1:5000, BAX (Abcam, ab32503) 1:1000; CytC (ab13575) 1:1000; Histone H3 (ab8580) 1:1000 NF-kB (ab32360 1:1000; Lamin B1 (ab16048) 1:1000; MTCO1 (ab14705) 1:1000. Membranes were washed in TBST (3 x 15 mins at RT) and then incubated with corresponding peroxidase-conjugated secondary antibodies (Dako, P0447, P0448) for 1h at RT. After further washing in TBST, blots were developed using an ECL Plus western blotting detection kit (Fisher Scientific, 12316992). Immunoreactive bands were analyzed by performing densitometry with ImageJ software.

Confocal Imaging/ImageJ*:* Fluorescent labeling was observed through a LSM 5 Pascal confocal microscope (Zeiss, Oberkochen, Germany) and images were recorded with the Pascal software (Zeiss). All image analysis was done using Fiji (ImageJ; NCBI, USA) and corresponding plug-ins. All staining was checked for non-specific antibody labeling using control samples without primary antibody. None of the controls showed any signs of nonspecific fluorescence. For ICC and IHC imaging, single optical sections were analyzed. The infiltrate analysis was done using orthogonal rendering 3D optical stacks and counting

the number of infiltrates per cell nucleus. The mitochondrial network analysis was performed using the 'skeletonize' plugin.

***Cell Proliferation assays**:* Cell proliferation assay were performed using the WST-1 Cell Proliferation Assay Kit (ab65473) and assessed on a standard plate reader (Tecan SUNRISE)

***Cell Death Assays**:* Cells were fixed in 4% PFA for 10 mins at, RT followed by 3 five-minute washes in PBS. Permeabilization was performed with 0.2% Triton-X100 in PBS for 10 mins at RT followed by washing. Death assays TUNEL Assay Kit - *in situ* Direct DNA Fragmentation (ab66108) as per the manufacturer's instructions. Alternatively, cells were live stained with Hoechst 33342 (Sigma H6024) and Propidium iodide (Sigma 25535) to mark apoptosing cells and imaged on an inverted fluorescence microscope.

***Fluorescence imaging**:* Cells were incubated with 5 μM dihydroethidium (DHE, Life Technologies, D-1168) or 5 μM MitoSOX (Life Technologies, M-36008) in recording media (125 mM NaCl, 5 mM KCl, 1 mM NaH_2PO_4, 20 mM HEPES, 5.5 mM glucose, 5 mM $NaHCO_3$, and 1 mM $CaCl_2$, pH 7.4) for 30 minutes at 37 ^{0}C. Cells were washed once in recording medium then transferred to a Leica SP-5 confocal microscope (63X oil objective lens) for imaging and fluorescence intensity was measured through continuous recording for at least 10 mins. Settings were kept constant between experiments. Mitochondrial ROIs were selected, and the corresponding fluorescence intensities calculated. For the transport of cholesterol assay, Ergosta (dehydroergosterol- ergosta-5,7,9(11),22-tetraen-3β-ol) was prepared and loaded as previously described [46]. Briefly, Ergosta was added to an aqueous solution of MβCD (3mM Ergosta and 30mM MβCD). This mixture was overlaid with nitrogen, continuously vortexed under light protection for 24 h at room temperature and filtered through a 0.2 μm filter to remove insoluble material and Ergosta crystals. Then, 20 μg of DHE was added to the cells in the form of DHE-MβCD complexes and allowed to incubate for 90 minutes at room temperature in PBS. Prior to imaging, cells were washed

three times with culture media before being incubated with 20 nM MitoTracker™ Red CMXRos. Cell were washed and then imaged.

Statistical analysis: Data are presented as mean ± standard deviation of the mean. One-way analysis of variance (ANOVA) was used in multiple group comparisons with Bonferroni's *post hoc* test to compare two data sets within the group and a *p* value less than 0.05 was considered significant. All analyses were performed in Microsoft Office Excel 2010 and GraphPad Prism 7. *p = <0.05, **p = <0.01, ***p = <0.001

Preparation of cells for Electron Microscopy (TEM and Immunogold TEM)

For TEM analysis, MDA-MB-231 cells (control and treated with 0.5 µm for 16 h) were fixed at room temperature with 2.5% glutaraldehyde (v/v) in 0.1 M sodium cacodylate buffer (pH 7.4) for 3 h. The cells were pelleted by centrifugation, washed in buffer and post-fixed for 1 h with 1% osmium tetroxide in 0.1 M sodium cacodylate buffer. Samples were thoroughly rinsed, dehydrated in a graded series of ethanols and embedded in epoxy resin (TAAB 812). Ultrathin sections (70-90 nm) were cut using a Leica UC7 ultramicrotome mounted on 150 mesh copper grids and contrasted using Uranyless (TAAB) and 3% Reynolds Lead citrate (TAAB). Sections were examined at 120kV on a JEOL JEM-1400Plus TEM fitted with a Ruby digital camera (2kx2k). For TEM immunogold labelling, cell samples were fixed with 4% (w/v) paraformaldehyde, 0.1% (v/v) glutaraldehyde in 0.1M phosphate buffer (pH 7.4) for 4 h at room temperature and spun down on 20% gelatine. Gelatine cell pellets were cryoprotected by incubating in 2.3M sucrose overnight at 4°C. Gelatine blocks containing cells were cut further into 1-2mm cubes, mounted on aluminium pins and cryofixed by plunging into liquid nitrogen. Samples were stored in liquid nitrogen prior to cryosectioning. Ultrathin sections (70-90 nm thick) were cut using a Leica EM FC6 cryo-ultramicrotome and mounted on pioloform film-supported nickel grids according to the Tokuyasu method (1). Sections were immunolabeled using anti-TSPO (Abcam, ab109497) (1:200) followed by a 12nm-colloidal gold anti-rabbit secondary antibody (Jackson ImmunoResearch) (1:40). Grids

were examined at 120 kV on a JEOL JEM-1400Plus TEM fitted with a Ruby digital camera (2kx2k).

Table 1: Half lifetime and diffusion distance of ROS

ROS	Half-Life	Diffusion distance
H_2O_2	500 s	1732 µm
OH^-	35 µs	4.58 µm
$O2^{--}$	10 ns	0.244 µm

Diffusion distance can be estimated by Einstein-Schomulochowski equation[41],

$\boxed{x = \sqrt{(6Dt)}}$ where *x* is the quadratic mean of the diffusion distance in 3-D space, *D* is the diffusion co-efficient, and *t* is the time, taken as the molecule half-life. A half-life is the time for a decrease in concentration of 1/*e* or 37%

Table 2: Chemical Structures of the Compounds Used

Compound	IUPAC	Structure
PK11195	1-(2-Chlorophenyl)-N-methyl-N-(1-methylpropyl)-3-isoquinolinecarboxamide;	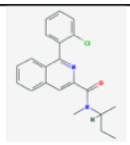
FGIN (FGIN-1-27)	N, N-Dihexyl-2-(4-fluorophenyl) indole-3-acetamide	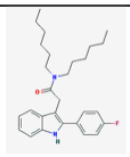
Ro5 (Ro5-4864)	7-chloro-5-(4-chlorophenyl)-1-methyl-3H-1,4-benzodiazepin-2-one	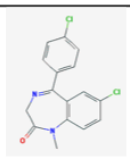
Staurosporine	(2S,3R,4R,6R)-3-methoxy-2-methyl-4-(methylamino)-29-oxa-1,7,17-triazaoctacyclo [12.12.2.1^{2,6}.0^{7,28}.0^{8,13}.0^{15,19}.0^{20,27}.0^{21,26}] nonacosa-8,10,12,14,19,21,23,25,27-nonaen-16-one	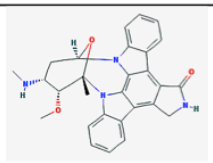
Doxorubicin	(7S,9S)-7-[(2R,4S,5S,6S)-4-amino-5-hydroxy-6-methyloxan-2-yl] oxy-6,9,11-trihydroxy-9-(2-hydroxyacetyl)-4-methoxy-8,10-dihydro-7H-tetracene-5,12-dione	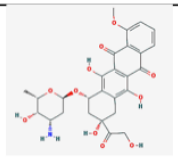
Vincristine	methyl (1R,9R,10S,11R,12R,19R)-11-(acetyloxy)-12-ethyl-4-[(13S,15S,17S)-17-ethyl-17-hydroxy-13-(methoxycarbonyl)-1,11-diazatetracyclo[13.3.1.0^{4},^{12}.0^{5},^{10}]nonadeca-4(12),5,7,9-tetraen-13-yl]-8-formyl-10-hydroxy-5-methoxy-8,16-diazapentacyclo[10.6.1.0^{1},^{9}.0^{2},^{7}.0^{16},^{19}]nonadeca-2,4,6,13-tetraene-10-carboxylate	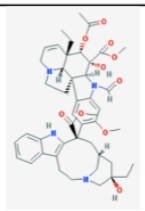
Tamoxifen	(2-{4-[(1Z)-1,2-diphenylbut-1-en-1-yl] phenoxy}ethyl)dimethylamine	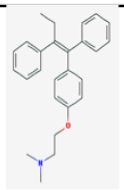

References

1 Nguyen, V. T. *et al.* Differential epigenetic reprogramming in response to specific endocrine therapies promotes cholesterol biosynthesis and cellular invasion. *Nat Commun* **6**, 10044, doi:10.1038/ncomms10044 (2015).

2 Magnani, L. *et al.* Acquired CYP19A1 amplification is an early specific mechanism of aromatase inhibitor resistance in ERalpha metastatic breast cancer. *Nat Genet* **49**, 444-450, doi:10.1038/ng.3773 (2017).

3 Hardwick, M. *et al.* Peripheral-type benzodiazepine receptor (PBR) in human breast cancer: correlation of breast cancer cell aggressive phenotype with PBR expression, nuclear localization, and PBR-mediated cell proliferation and nuclear transport of cholesterol. *Cancer Res* **59**, 831-842 (1999).

4 Guha, M. *et al.* Mitochondrial retrograde signaling induces epithelial-mesenchymal transition and generates breast cancer stem cells. *Oncogene* **33**, 5238-5250, doi:10.1038/onc.2013.467 (2014).

5 Carden, T., Singh, B., Mooga, V., Bajpai, P. & Singh, K. K. Epigenetic modification of miR-663 controls mitochondria-to-nucleus retrograde signaling and tumor progression. *J Biol Chem*, doi:10.1074/jbc.M117.797001 (2017).

6 Fan, J. & Papadopoulos, V. Evolutionary origin of the mitochondrial cholesterol transport machinery reveals a universal mechanism of steroid hormone biosynthesis in animals. *PLoS One* **8**, e76701, doi:10.1371/journal.pone.0076701 (2013).

7 Quiros, P. M., Mottis, A. & Auwerx, J. Mitonuclear communication in homeostasis and stress. *Nat Rev Mol Cell Biol* **17**, 213-226, doi:10.1038/nrm.2016.23 (2016).

8 De Stefani, D. *et al.* VDAC1 selectively transfers apoptotic Ca2+ signals to mitochondria. *Cell Death Differ* **19**, 267-273, doi:10.1038/cdd.2011.92 (2012).

9 Wallace, D. C. Mitochondria and cancer. *Nat Rev Cancer* **12**, 685-698, doi:10.1038/nrc3365 (2012).

10 Rizzuto, R., De Stefani, D., Raffaello, A. & Mammucari, C. Mitochondria as sensors and regulators of calcium signalling. *Nat Rev Mol Cell Biol* **13**, 566-578, doi:10.1038/nrm3412 (2012).

11 Monaghan, R. M. *et al.* A nuclear role for the respiratory enzyme CLK-1 in regulating mitochondrial stress responses and longevity. *Nat Cell Biol* **17**, 782-792, doi:10.1038/ncb3170 (2015).

12 Tu, B. P. & McKnight, S. L. Metabolic cycles as an underlying basis of biological oscillations. *Nature reviews. Molecular cell biology* **7**, 696-701, doi:10.1038/nrm1980 (2006).

13 Bonuccelli, G. *et al.* Ketones and lactate "fuel" tumor growth and metastasis: Evidence that epithelial cancer cells use oxidative mitochondrial metabolism. *Cell cycle* **9**, 3506-3514 (2010).

14 Pavlides, S. *et al.* The reverse Warburg effect: aerobic glycolysis in cancer associated fibroblasts and the tumor stroma. *Cell cycle* **8**, 3984-4001 (2009).

15 Miettinen, H. *et al.* Expression of peripheral-type benzodiazepine receptor and diazepam binding inhibitor in human astrocytomas: relationship to cell proliferation. *Cancer Res* **55**, 2691-2695 (1995).

16 Beinlich, A., Strohmeier, R., Kaufmann, M. & Kuhl, H. Relation of cell proliferation to expression of peripheral benzodiazepine receptors in human breast cancer cell lines. *Biochem Pharmacol* **60**, 397-402 (2000).

17 Maaser, K. *et al.* Up-regulation of the peripheral benzodiazepine receptor during human colorectal carcinogenesis and tumor spread. *Clin Cancer Res* **11**, 1751-1756, doi:10.1158/1078-0432.CCR-04-1955 (2005).

18 Rone, M. B., Fan, J. & Papadopoulos, V. Cholesterol transport in steroid biosynthesis: role of protein-protein interactions and implications in disease states. *Biochim Biophys Acta* **1791**, 646-658, doi:10.1016/j.bbalip.2009.03.001 (2009).

19 Rone, M. B. *et al.* Identification of a dynamic mitochondrial protein complex driving cholesterol import, trafficking, and metabolism to steroid hormones. *Mol Endocrinol* **26**, 1868-1882, doi:10.1210/me.2012-1159 (2012).

20 Papadopoulos, V. *et al.* Translocator protein-mediated pharmacology of cholesterol transport and steroidogenesis. *Mol Cell Endocrinol* **408**, 90-98, doi:10.1016/j.mce.2015.03.014 (2015).

21 Gatliff, J. & Campanella, M. TSPO is a REDOX regulator of cell mitophagy. *Biochem Soc Trans* **43**, 543-552, doi:10.1042/BST20150037 (2015).

22 Gatliff, J. *et al.* TSPO interacts with VDAC1 and triggers a ROS-mediated inhibition of mitochondrial quality control. *Autophagy* **10**, 2279-2296, doi:10.4161/15548627.2014.991665 (2014).

23 Gatliff, J. *et al.* A role for TSPO in mitochondrial Ca(2+) homeostasis and redox stress signaling. *Cell Death Dis* **8**, e2896, doi:10.1038/cddis.2017.186 (2017).

24 Zheng, J. *et al.* Differential expression of the 18 kDa translocator protein (TSPO) by neoplastic and inflammatory cells in mouse tumors of breast cancer. *Mol Pharm* **8**, 823-832, doi:10.1021/mp100433c (2011).

25 Gatliff, J. & Campanella, M. The 18 kDa translocator protein (TSPO): a new perspective in mitochondrial biology. *Current molecular medicine* **12**, 356-368 (2012).

26 Tang, D. *et al.* Preclinical Evaluation of a Novel TSPO PET Ligand 2-(7-Butyl-2-(4-(2-[(18)F]Fluoroethoxy)phenyl)-5-Methylpyrazolo[1,5-a]Pyrimidin-3 -yl)-N,N-Diethylacetamide ((18)F-VUIIS1018A) to Image Glioma. *Mol Imaging Biol*, doi:10.1007/s11307-018-1198-7 (2018).

27 Tantawy, M. N. *et al.* Translocator Protein PET Imaging in a Preclinical Prostate Cancer Model. *Mol Imaging Biol* **20**, 200-204, doi:10.1007/s11307-017-1113-7 (2018).

28 Herrero-Martin, G. & Lopez-Rivas, A. Statins activate a mitochondria-operated pathway of apoptosis in breast tumor cells by a mechanism regulated by ErbB2 and dependent on the prenylation of proteins. *FEBS Lett* **582**, 2589-2594, doi:10.1016/j.febslet.2008.06.034 (2008).

29 Khan, S., Lopez-Dee, Z., Kumar, R. & Ling, J. Activation of NFkB is a novel mechanism of pro-survival activity of glucocorticoids in breast cancer cells. *Cancer Lett* **337**, 90-95, doi:10.1016/j.canlet.2013.05.020 (2013).

30 Ling, J. & Kumar, R. Crosstalk between NFkB and glucocorticoid signaling: a potential target of breast cancer therapy. *Cancer Lett* **322**, 119-126, doi:10.1016/j.canlet.2012.02.033 (2012).

31 East, D. A. *et al.* PMI: a DeltaPsim independent pharmacological regulator of mitophagy. *Chem Biol* **21**, 1585-1596, doi:10.1016/j.chembiol.2014.09.019 (2014).

32 Georgakopoulos, N. D. *et al.* Reversible Keap1 inhibitors are preferential pharmacological tools to modulate cellular mitophagy. *Sci Rep* **7**, 10303, doi:10.1038/s41598-017-07679-7 (2017).

33 Jaremko, L., Jaremko, M., Giller, K., Becker, S. & Zweckstetter, M. Structure of the mitochondrial translocator protein in complex with a diagnostic ligand. *Science* **343**, 1363-1366, doi:10.1126/science.1248725 (2014).

34 Jeng, M. H. *et al.* Estrogen receptor expression and function in long-term estrogen-deprived human breast cancer cells. *Endocrinology* **139**, 4164-4174, doi:10.1210/endo.139.10.6229 (1998).

35 Santen, R. J., Lobenhofer, E. K., Afshari, C. A., Bao, Y. & Song, R. X. Adaptation of estrogen-regulated genes in long-term estradiol deprived MCF-7 breast cancer cells. *Breast Cancer Res Treat* **94**, 213-223, doi:10.1007/s10549-005-5776-4 (2005).

36 Ishikawa, K. *et al.* ROS-generating mitochondrial DNA mutations can regulate tumor cell metastasis. *Science* **320**, 661-664, doi:10.1126/science.1156906 (2008).

37 Marwarha, G., Raza, S., Hammer, K. & Ghribi, O. 27-hydroxycholesterol: A novel player in molecular carcinogenesis of breast and prostate cancer. *Chem Phys Lipids* **207**, 108-126, doi:10.1016/j.chemphyslip.2017.05.012 (2017).

38 Kloudova, A., Guengerich, F. P. & Soucek, P. The Role of Oxysterols in Human Cancer. *Trends Endocrinol Metab* **28**, 485-496, doi:10.1016/j.tem.2017.03.002 (2017).

39 Modzel, M., Lund, F. W. & Wustner, D. Synthesis and Live-Cell Imaging of Fluorescent Sterols for Analysis of Intracellular Cholesterol Transport. *Methods Mol Biol* **1583**, 111-140, doi:10.1007/978-1-4939-6875-6_10 (2017).

40 Bovenga, F., Sabba, C. & Moschetta, A. Uncoupling nuclear receptor LXR and cholesterol metabolism in cancer. *Cell Metab* **21**, 517-526, doi:10.1016/j.cmet.2015.03.002 (2015).

41 Cardoso, A. R. *et al.* Mitochondrial compartmentalization of redox processes. *Free Radic Biol Med* **52**, 2201-2208, doi:10.1016/j.freeradbiomed.2012.03.008 (2012).

42 Spencer, W. *et al.* Taxol selectively blocks microtubule dependent NF-kappaB activation by phorbol ester via inhibition of IkappaBalpha phosphorylation and degradation. *Oncogene* **18**, 495-505, doi:10.1038/sj.onc.1202335 (1999).

43 Becker-Weimann, S. *et al.* NFkB disrupts tissue polarity in 3D by preventing integration of microenvironmental signals. *Oncotarget* **4**, 2010-2020, doi:10.18632/oncotarget.1451 (2013).

44 Bussolati, G., Marchio, C., Gaetano, L., Lupo, R. & Sapino, A. Pleomorphism of the nuclear envelope in breast cancer: a new approach to an old problem. *J Cell Mol Med* **12**, 209-218, doi:10.1111/j.1582-4934.2007.00176.x (2008).

45 Morelli, A. *et al.* Extracellular ATP causes ROCK I-dependent bleb formation in P2X7-transfected HEK293 cells. *Mol Biol Cell* **14**, 2655-2664, doi:10.1091/mbc.02-04-0061 (2003).

46 McIntosh, A. L. *et al.* Fluorescence techniques using dehydroergosterol to study cholesterol trafficking. *Lipids* **43**, 1185-1208, doi:10.1007/s11745-008-3194-1 (2008).

Figure 1

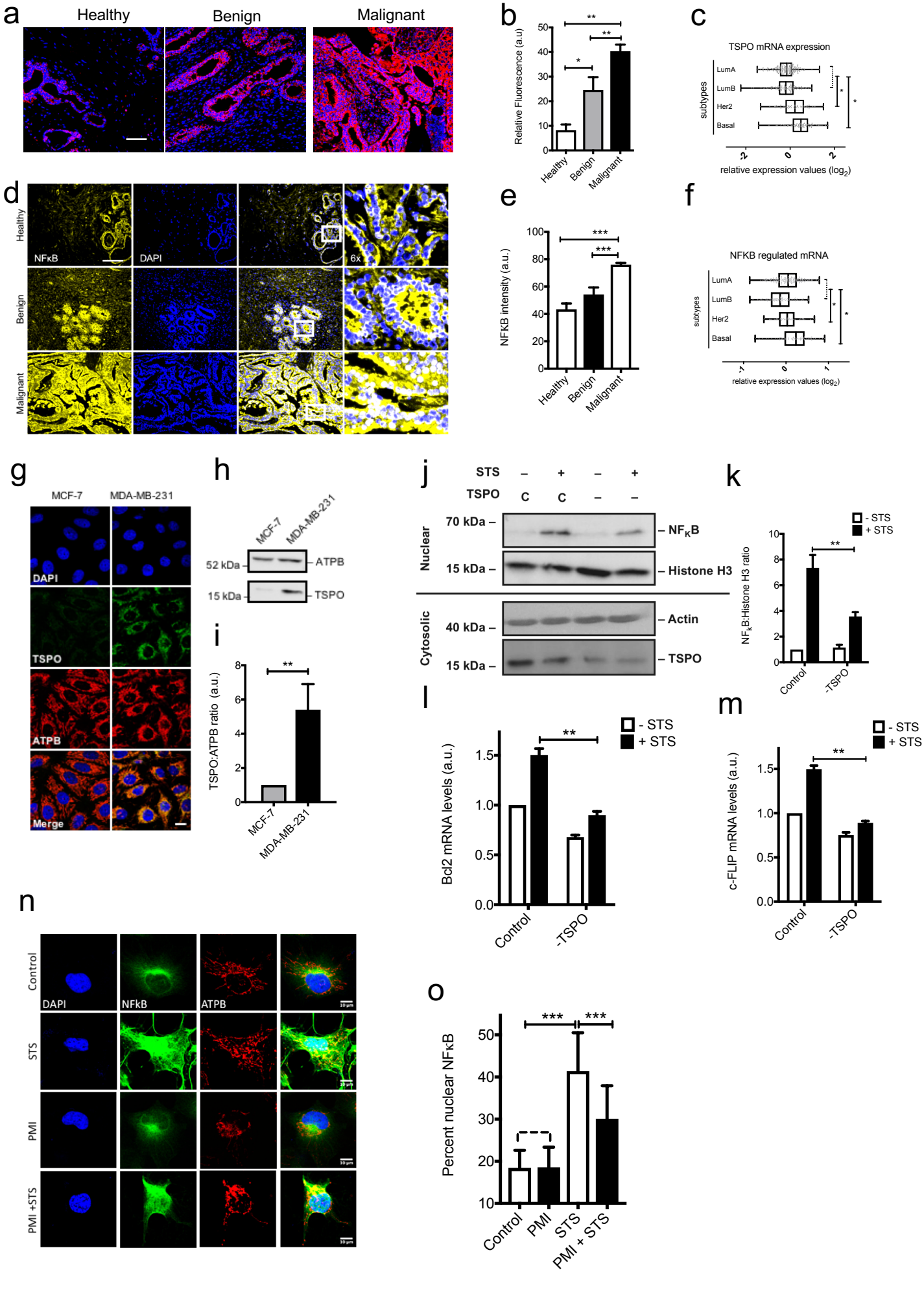
a
Healthy
Benign
Malignant
b
Relative Fluorescence (a.u)
Healthy
Benign
Malignant
c
TSPO mRNA expression
subtypes
LumA
LumB
Her2
Basal
relative expression values (log2)
d
Healthy
Benign
Malignant
NFκB
DAPI
6x
e
NFKB intensity (a.u.)
f
NFKB regulated mRNA
g
MCF-7
MDA-MB-231
DAPI
TSPO
ATPB
Merge
h
52 kDa
ATPB
15 kDa
TSPO
i
TSPO:ATPB ratio (a.u.)
j
STS
TSPO
Nuclear
70 kDa
NFκB
15 kDa
Histone H3
Cytosolic
40 kDa
Actin
15 kDa
TSPO
k
NFκB:Histone H3 ratio
- STS
+ STS
Control
-TSPO
l
Bcl2 mRNA levels (a.u.)
m
c-FLIP mRNA levels (a.u.)
n
Control
STS
PMI
PMI +STS
DAPI
NFkB
ATPB
o
Percent nuclear NFκB
Control
PMI
STS
PMI + STS

Figure 2

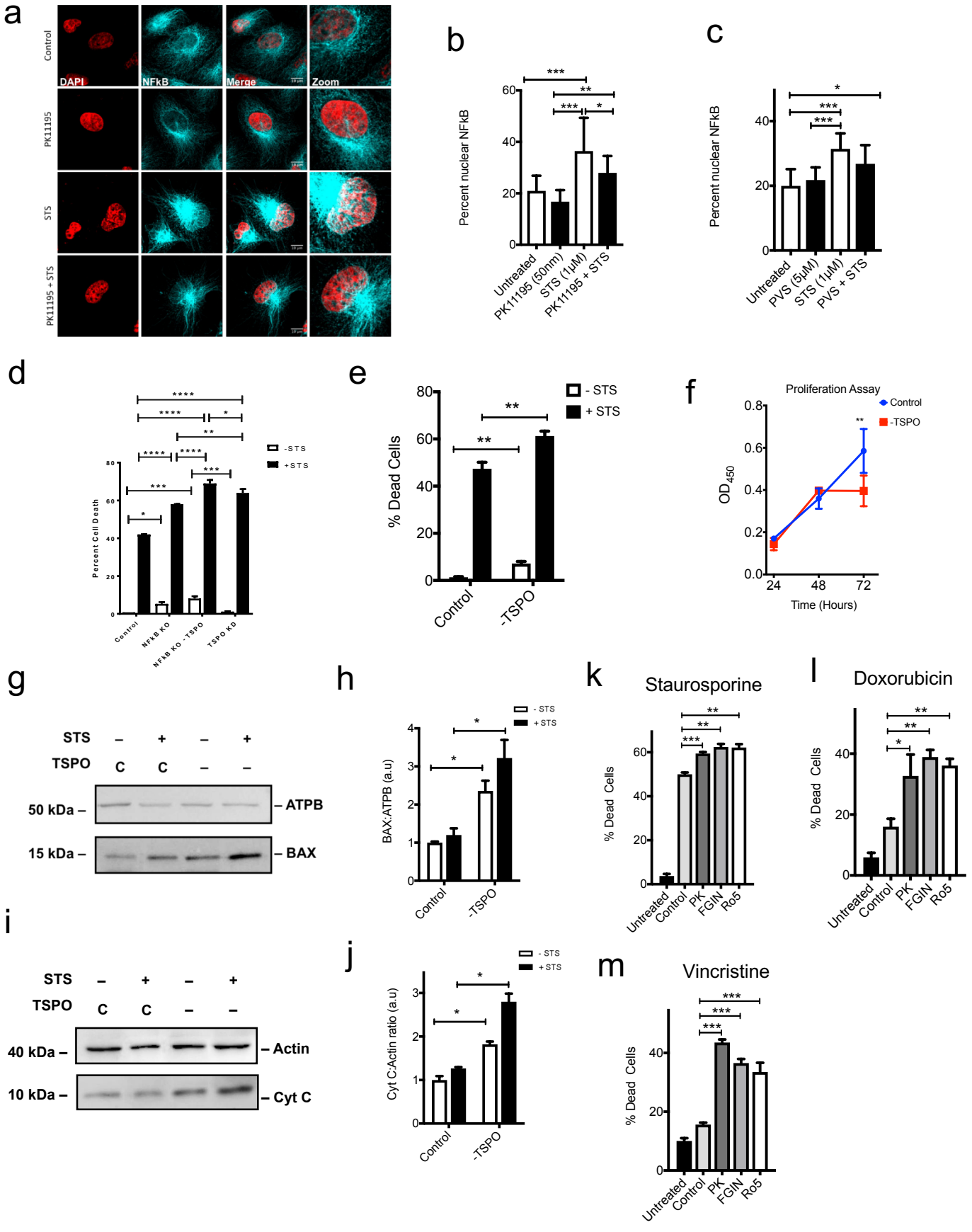
a
Control
PK11195
STS
PK11195 + STS
DAPI
NFkB
Merge
Zoom
b
Percent nuclear NFkB
Untreated
PK11195 (50nm)
STS (1μM)
PK11195 + STS
c
Percent nuclear NFkB
Untreated
PVS (5μM)
STS (1μM)
PVS + STS
d
Percent Cell Death
-STS
+STS
Control
NFkB KO
NFkB KO -TSPO
TSPO KD
e
% Dead Cells
- STS
+ STS
Control
-TSPO
f
Proliferation Assay
Control
-TSPO
OD450
Time (Hours)
g
STS
TSPO
50 kDa –
– ATPB
15 kDa –
– BAX
h
BAX:ATPB (a.u)
- STS
+ STS
Control
-TSPO
i
STS
TSPO
40 kDa –
– Actin
10 kDa –
– Cyt C
j
Cyt C:Actin ratio (a.u)
- STS
+ STS
Control
-TSPO
k
Staurosporine
% Dead Cells
Untreated
Control
PK
FGIN
Ro5
l
Doxorubicin
% Dead Cells
Untreated
Control
PK
FGIN
Ro5
m
Vincristine
% Dead Cells
Untreated
Control
PK
FGIN
Ro5

Figure 3

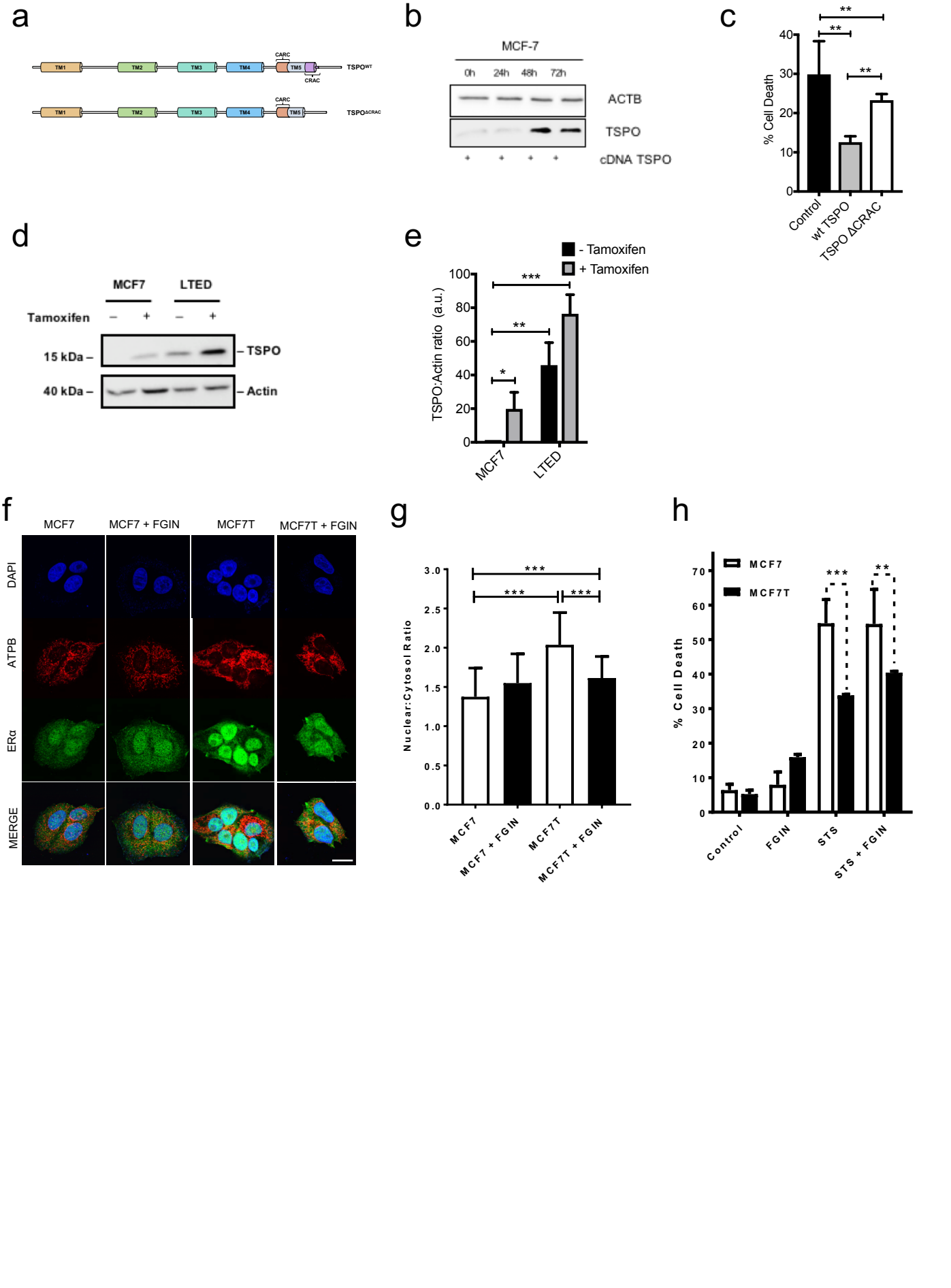
a
TM1
TM2
TM3
TM4
TM5
CARC
CRAC
TSPOWT
TSPOΔCRAC
b
MCF-7
0h
24h
48h
72h
ACTB
TSPO
cDNA TSPO
c
% Cell Death
Control
wt TSPO
TSPO ΔCRAC
d
MCF7
LTED
Tamoxifen
15 kDa –
– TSPO
40 kDa –
– Actin
e
- Tamoxifen
+ Tamoxifen
TSPO:Actin ratio (a.u.)
MCF7
LTED
f
MCF7
MCF7 + FGIN
MCF7T
MCF7T + FGIN
DAPI
ATPB
ERα
MERGE
g
Nuclear:Cytosol Ratio
MCF7
MCF7 + FGIN
MCF7T
MCF7T + FGIN
h
MCF7
MCF7T
% Cell Death
Control
FGIN
STS
STS + FGIN

Figure 4

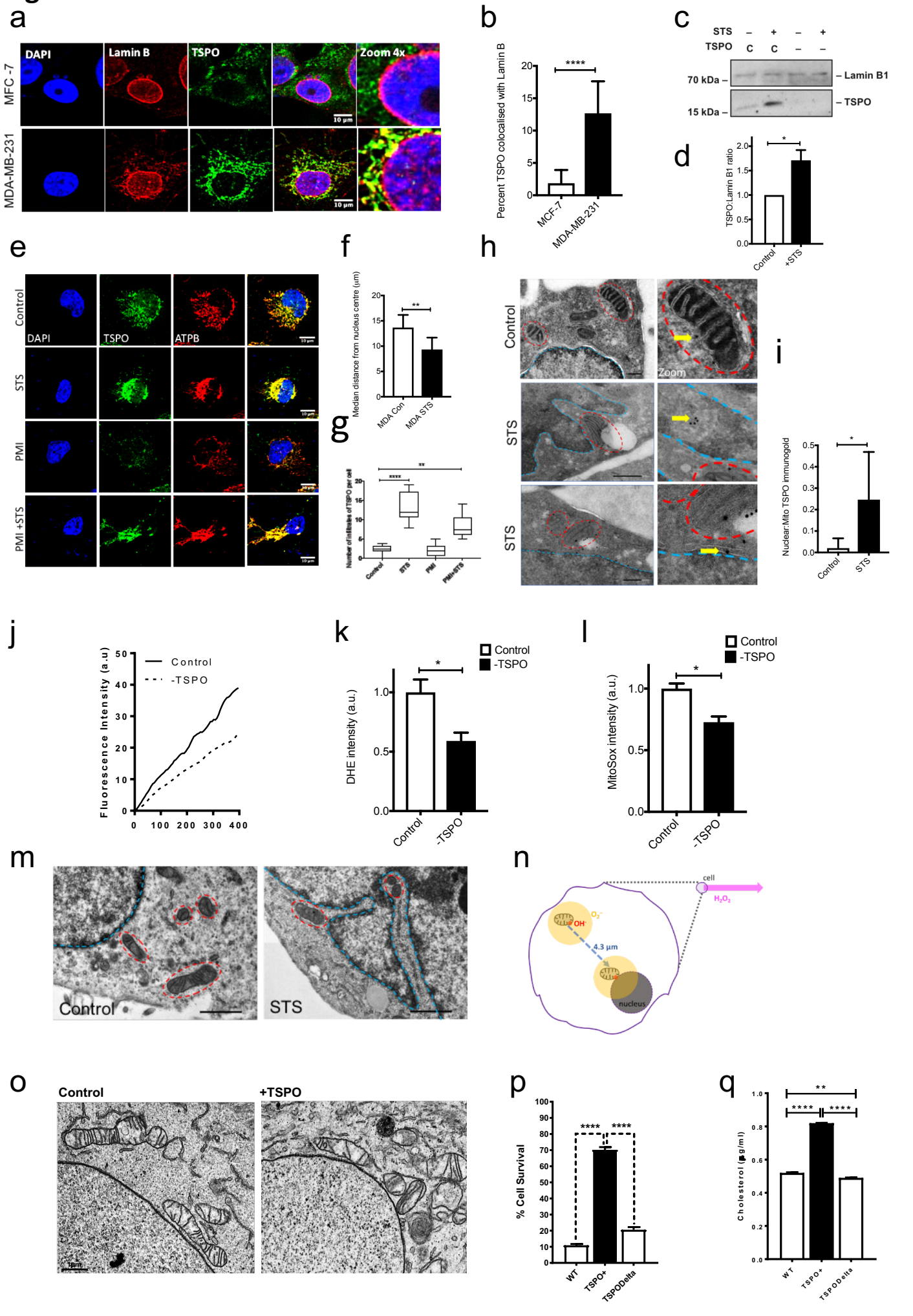
a
DAPI
Lamin B
TSPO
Zoom 4x
MFC -7
MDA-MB-231
10 µm
b
Percent TSPO colocalised with Lamin B
****
MCF-7
MDA-MB-231
c
STS – + – +
TSPO C C – –
70 kDa –
15 kDa –
– Lamin B1
– TSPO
d
TSPO:Lamin B1 ratio
*
Control
+STS
e
Control
STS
PMI
PMI +STS
DAPI
TSPO
ATPB
f
Median distance from nucleus centre (µm)
**
MDA Con
MDA STS
g
Number of inclusions of TSPO per cell
****
**
Control
STS
PMI
PMI+STS
h
Control
STS
STS
Zoom
i
Nuclear:Mito TSPO immunogold
*
Control
STS
j
Fluorescence Intensity (a.u)
Control
-TSPO
k
DHE intensity (a.u.)
Control
-TSPO
*
l
MitoSox intensity (a.u.)
Control
-TSPO
*
m
Control
STS
n
cell
H_2O_2
$O_2^{\cdot-}$
$OH^{\cdot}$
4.3 µm
nucleus
o
Control
+TSPO
1µm
p
% Cell Survival
****
****
WT
TSPO+
TSPODelta
q
Cholesterol (µg/ml)
**
****
****
WT
TSPO+
TSPODelta

Figure 5

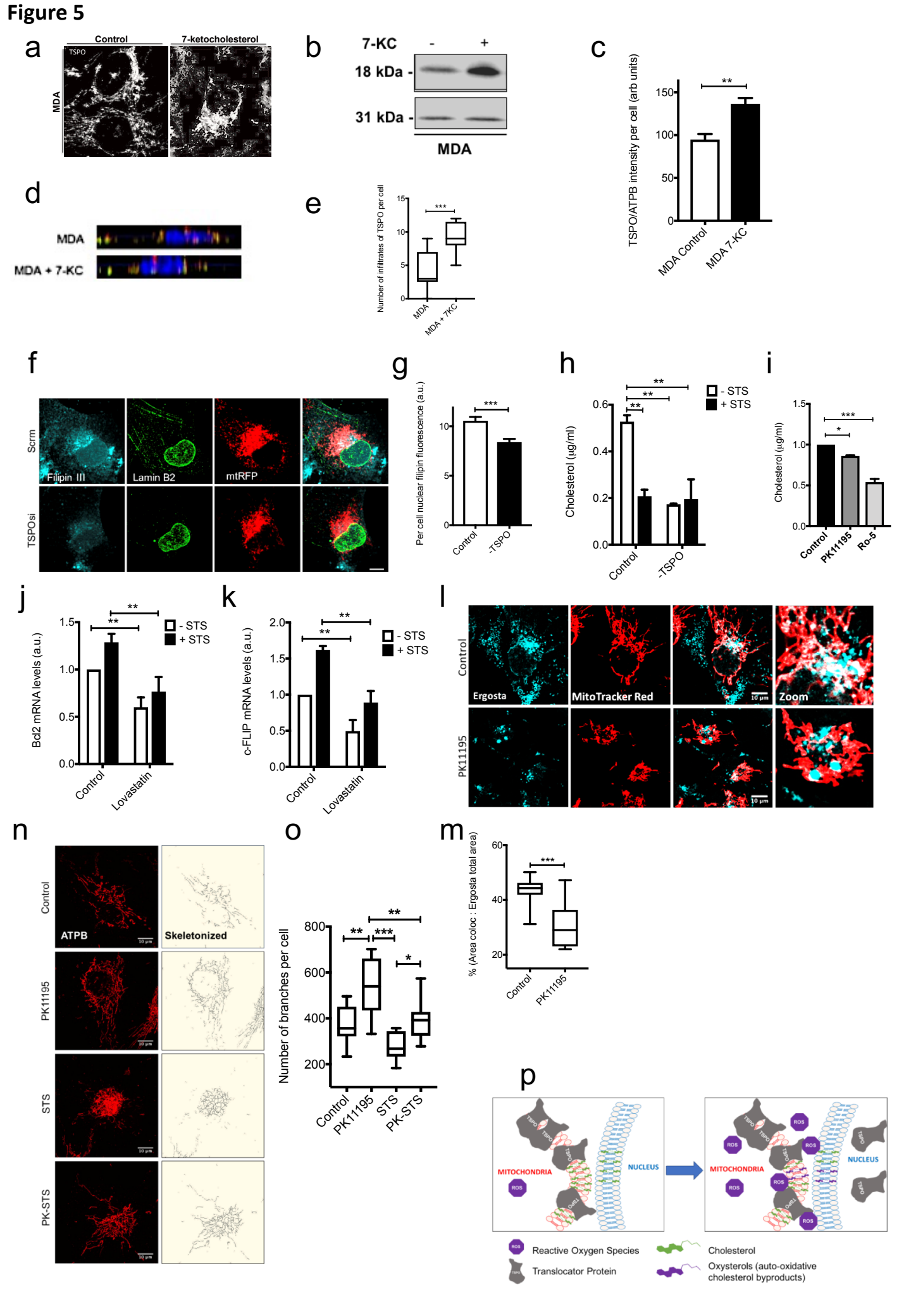
a
Control
7-ketocholesterol
TSPO
MDA
b
7-KC
-
+
18 kDa -
31 kDa -
MDA
c
TSPO/ATPB intensity per cell (arb units)
150
100
50
0
**
MDA Control
MDA 7-KC
d
MDA
MDA + 7-KC
e
Number of infiltrates of TSPO per cell
15
10
5
0
***
MDA
MDA + 7KC
f
Scrm
TSPOsi
Filipin III
Lamin B2
mtRFP
g
Per cell nuclear filipin fluorescence (a.u.)
10
5
0
***
Control
-TSPO
h
Cholesterol (µg/ml)
0.6
0.4
0.2
0.0
**
**
**
- STS
+ STS
Control
-TSPO
i
Cholesterol (µg/ml)
1.5
1.0
0.5
0.0
***
*
Control
PK11195
Ro-5
j
Bcl2 mRNA levels (a.u.)
1.5
1.0
0.5
0.0
**
**
- STS
+ STS
Control
Lovastatin
k
c-FLIP mRNA levels (a.u.)
2.0
1.5
1.0
0.5
0.0
**
**
- STS
+ STS
Control
Lovastatin
l
Control
PK11195
Ergosta
MitoTracker Red
Zoom
10 µm
n
Control
PK11195
STS
PK-STS
ATPB
Skeletonized
10 µm
o
Number of branches per cell
800
600
400
200
**
**
***
*
Control
PK11195
STS
PK-STS
m
% (Area coloc : Ergosta total area)
60
40
20
***
Control
PK11195
p
MITOCHONDRIA
NUCLEUS
ROS
TSPO
Reactive Oxygen Species
Translocator Protein
Cholesterol
Oxysterols (auto-oxidative cholesterol byproducts)